Photosynthesis-Induced Biofilm Calcification and Calcium Concentrations in Phanerozoic Oceans

Gernot Arp,* Andreas Reimer, Joachim Reitner

Photosynthetic carbon assimilation is commonly invoked as the cause of calcium carbonate precipitation in cyanobacterial biofilms that results in the formation of calcareous stromatolites. However, biofilm calcification patterns in recent lakes and simulation of photosynthetically induced rise in calcium carbonate supersaturation demonstrate that this mechanism applies only in settings low in dissolved inorganic carbon and high in calcium. Taking into account paleo–partial pressure curves for carbon dioxide, we show that Phanerozoic oceans sustaining calcified cyanobacteria must have had considerably higher calcium concentrations than oceans of today. In turn, the enigmatic lack of calcified cyanobacteria in stromatolite-bearing Precambrian sequences can now be explained as a result of high dissolved inorganic carbon concentrations.

There is increasing evidence that the ocean's chemical composition fluctuated considerably during the Precambrian as well as during the Phanerozoic (*1–3*). Conditions favoring carbonate precipitation can be inferred from cyanobacteria, because their calcification is dependent on the supersaturation of the ambient water with respect to $CaCO_3$ minerals (*4*, *5*). Recurrent calcification of microbial mats and biofilms, commonly dominated by cyanobacteria and/or nonphototrophic bacteria, leads to the formation of stromatolites, laminated reeflike structures that once were common in the marine realm. Starting with a limited number of Archean occurrences, stromatolites were most widespread and abundant in the Proterozoic, followed by a severe decline in the latest Proterozoic (*6*, *7*). Subsequently, clotted microbial deposits, so-called thrombolites, were common since the beginning of the Cambrian, but finally vanished almost completely from normal-marine environments during the Late Cretaceous, together with the remaining stromatolites (*8*).

Carbonate stromatolites of the Precambrian almost never exhibit tubular or vesicular carbonate microfossils of cyanobacteria, which should have been the dominant group of microorganisms in most of the shallow-marine stromatolite occurrences (*8*, *9*). This appears enigmatic (*9*) because cyanobacterial filament and cell remains have been preserved when early silicification occurred (*10*). On the other hand, such calcified cyanobacteria occur nearly continuously in fluctuating abundances from the Cambrian to the Cretaceous, either forming skeletal stromatolites, oncolites, or distinct microfossils such as *Girvanella* (*10*).

Three crucial steps in cyanobacterial biofilm calcification can be distinguished: (i) the initial supersaturation of the macroenvironment with regard to $CaCO_3$ minerals, (ii) the shift of the carbonate equilibrium to surpass the critical supersaturation for $CaCO_3$ mineral formation, and (iii) the process of seed crystal formation. In the following, saturation is given by the saturation index

$$\mathrm{SI}_{\mathrm{SO}} = \log(\mathrm{IAP}/K_{\mathrm{SO}}) \qquad (1)$$

where IAP denotes the ion activity product and K_{SO} is the solubility product of the corresponding mineral (solid phase) (*11*). Case studies of nonmarine settings exhibiting present-day calcifying cyanobacterial biofilms indicate a 9.5- to 15-fold supersaturation of the ambient water with respect to calcite (*12–14*). Therefore, an ~10-fold supersaturation ($\mathrm{SI}_{\mathrm{Cc}} = 1.0$) is here taken as a prerequisite for cyanobacterial calcification.

$CaCO_3$ mineral nucleation in microbial biofilms always starts from the common gel-like exopolymer matrix. Apart from their biological functions (*15*), extracellular polymeric substances (EPS), arranged in a highly hydrated network, affect mineralization in two ways. (i) They permit the establishment of physicochemical and chemical microgradients by reducing diffusion rates, and (ii) they bind divalent cations such as Ca^{2+} and Mg^{2+} from the liquid phase. The latter reflects the abundance of acidic groups within the EPS, which is not merely a sticky mass trapping and binding particles, but is composed largely of highly reactive, carboxylated polysaccharides (*15*, *16*). In accordance with the concept of organic matrix–mediated biomineralization (*17*, *18*), the stereochemical arrangement of these acidic groups is of crucial importance in mineral nucleation. Highly ordered acidic groups at defined distances that correspond to the crystal lattice promote nucleation, whereas irregularly arranged groups inhibit precipitation. Because EPS are, in contrast to organic matrices in biomineralization, highly diverse and disordered, this latter effect prevails in biofilms. Nucleation of $CaCO_3$ only occurs at acidic groups, which are suitably arranged mainly by accident, after a sufficient diffusive Ca^{2+} supply surpasses the complexation capacity of the EPS. As a result, if no effective physicochemical microgradients are established by the microorganisms, randomly distributed crystals form in the EPS (*19*).

Stimulated by the hypothesis (*20*) that ocean chemistry before 1000 Ma (million years ago) might have been highly alkaline, with pH values up to 10, and that soda lake microbialites may have Proterozoic counterparts, we investigated biofilm mineralization in soda lakes. Typically, physicochemically driven $CaCO_3$ precipitation of randomly distributed crystals occurs in the biofilm EPS at the contact to the supersaturated liquid phase so that no defined sheath impregnation results (*12–14*, *19*).

By contrast, for the formation of calcified cyanobacteria, it is critical that photosynthetic carbon withdrawl creates a pH-microgradient within the trichome-surrounding sheath to induce a spatially defined $CaCO_3$ impregnation (*19*). A causal relation of photosynthetic carbon assimilation and carbonate precipitation in cyanobacteria has been shown convincingly for freshwater settings, both by isotopic and experimental studies (*21*, *22*). So, how strong is the relative effect of photosynthesis in shifting carbonate equilibrium in the different hydrochemical settings?

The basic concept is expressed by the solubility product

$$K_{\mathrm{SO}} = \{Ca^{2+}\} \times \{CO_3^{2-}\} \qquad (2)$$

A rise in the concentration of CO_3^{2-} ($[CO_3^{2-}]$) will cause the ion activity product to exceed the solubility product, resulting in higher supersaturation the lower the initial concentration in dissolved inorganic carbon (DIC) is. In the case of photosynthesis, the rise in $[CO_3^{2-}]$ results from the disproportionation of bicarbonate to carbonate and CO_2, which is fixed by the organisms (*23*):

$$2HCO_3^- \rightleftharpoons CO_3^{2-} + CO_2 + H_2O \qquad (3)$$

To simulate the susceptibility of calcite supersaturation of high-Ca^{2+}/low-DIC and low-Ca^{2+}/high-DIC waters against a given photosynthetic carbon removal, we calculated model curves (*24*). The same procedure was applied to water-chemistry data of 29

Göttinger Zentrum für Geowissenschaften, Abteilung Geobiologie, Universität Göttingen, Goldschmidtstrasse 3, D-37077 Göttingen, Germany.

*To whom correspondence should be addressed. E-mail: garp@gwdg.de

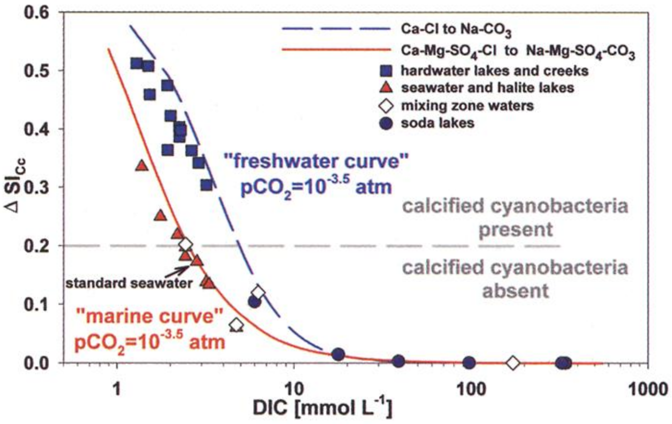

Fig. 1. Computed microenvironmental rise in the calcite supersaturation index (ΔSI_{Cc}) of natural waters (*24*) upon a carbon decrease by 200 μmol liter^{-1} as a function of DIC for present-day atmospheric pCO$_2$ = $10^{-3.5}$ atm. ΔSI_{Cc} = 0 corresponds to an initial 10-fold calcite supersaturation necessary for any cyanobacterial biofilm calcification.

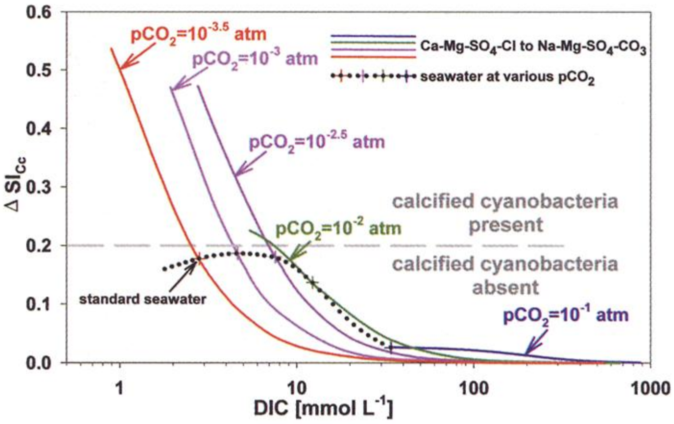

Fig. 2. Computed rise in the calcite supersaturation index (ΔSI_{Cc}) of marine waters upon a carbon removal of 200 μmol liter^{-1} as a function of DIC at various values of pCO$_2$. Calculations are based on a supposed 10-fold initial supersaturation (ΔSI_{Cc} = 0). The rise in supersaturation refers only to the microenvironment surrounding cyanobacterial cells, not the whole ocean.

settings sustaining calcifying biofilms (*24*). The resulting difference between the calcite supersaturation index before and after carbon subtraction, termed ΔSI_{Cc}, is plotted against DIC at equilibrium conditions in Fig. 1.

As a result, high-DIC waters—i.e., soda lakes and adjacent mixing zones at freshwater inputs—show a negligible to minor rise in calcite supersaturation upon carbon removal (Fig. 1). This is because of the large carbon pool and the strong pH buffering of soda lake waters. All of these high-DIC settings lack CaCO$_3$ precipitates spatially linked to cyanobacterial sheaths (*25*). Low-DIC marine settings and Na-Cl–dominated lakes show minor to moderately high ΔSI_{Cc} values. Lake Tanganyika (Tanzania), Lake Satonda (Indonesia), Lake Thetis, and Shark Bay (Western Australia) cluster between 0.1 and 0.2 ΔSI_{Cc}. These settings, which presently sustain microbial reef growth, show clotted, microcrystalline precipitates within the cyanobacterial biofilm EPS (*25*). Nonetheless, precipitates immediately linked to cyanobacteria occur regularly in Lake Clifton (Western Australia) at a ΔSI_{Cc} of 0.20, although a clotted fabric still dominates in these thrombolites (*25*). Thus, a ΔSI_{Cc} of at least 0.20 is here considered necessary for the formation of calcified cyanobacteria as defined by CaCO$_3$-impregnated cyanobacterial sheaths. Saline pools of the Aldabra atoll (Seychelles) (ΔSI_{Cc} = 0.18 − 0.30) exhibit stromatolites that locally contain cyanobacterial filament moulds encased in microcrystalline carbonate (*25*). Riding (*26*) described calcareous sheath impregnation in *Plectonema* from another pool on Aldabra high in Ca^{2+} as a possible analog of the calcified cyanobacterium *Girvanella*.

Low-DIC nonmarine settings—i.e., hardwater lakes and creeks—show a relatively strong rise in calcite supersaturation upon DIC removal (ΔSI_{Cc} = 0.3 − 0.5). The ΔSI_{Cc} is generally higher compared with marine water of the same initial DIC (Fig. 1) where Mg^{2+} and SO$_4{}^{2-}$ tend to lower free Ca^{2+} and CO$_3{}^{2-}$ concentrations as a result of ion pairing and complexation. Commonly, physicochemical CO$_2$ degassing dominates in hardwater creeks, and cyanobacterial filaments mineralize externally (*4*, *6*). Only when in equilibrium with atmospheric pCO$_2$ does sheath impregnation by microcrystalline carbonate occur. Notably, the few known case studies of proven photosynthesis-induced CaCO$_3$ precipitation show the most substantial calculated rise in supersaturation upon DIC removal (Fig. 1): Fayetteville Green Lake (*21*) and a pond from the Everglades (*22*).

Figure 2 demonstrates the photosynthetic effect on supersaturation at pCO$_2$ levels expected for certain periods in Earth's history. Whereas high ΔSI_{Cc} values (>0.20) can be achieved for a pCO$_2$ between 10^{-3} and $10^{-2.5}$ atm, if sufficient Ca^{2+} is added, at higher pCO$_2$ (10^{-2}, 10^{-1} atm) ΔSI_{Cc} generally remains below this threshold, and calcified cyanobacteria are unlikely to occur. The dotted line in Fig. 2 illustrates the susceptibility of standard seawater to carbon removal by rising pCO$_2$ at a constantly held 10-fold initial supersaturation. After reaching a maximum ΔSI_{Cc} at pCO$_2$ = 10^{-3} atm, standard marine waters show an increasingly low reaction to carbon removal at higher pCO$_2$ conditions. In any case, only an additional Ca^{2+} input can cause the ΔSI_{Cc} of seawater to exceed the threshold for cyanobacterial sheath calcification of 0.20.

As a result of this effect, a lower threshold of Ca^{2+} concentrations can be calculated for Phanerozoic oceans that sustained calcified cyanobacteria (Fig. 3). Accepting palaeo-pCO$_2$ curves of Berner (*27*) and Ekart *et al.* (*28*) and a ΔSI_{Cc} of 0.20 to enable CaCO$_3$ impregnation of cyanobacterial sheaths by photosynthesis, at least 13 mmol liter^{-1} Ca^{2+} were necessary to sustain calcified cyanobacteria in Carboniferous to recent oceans. Earlier in the Paleozoic, Ca^{2+} concentrations up to at least 23 mmol liter^{-1} must be assumed.

The resulting Ca^{2+} minimum concentrations are compared with the Ca^{2+} concentrations derived from model calculations by Stanley and Hardie (*2*) (Fig. 3A), which are based on steady-state mixing of river water and mid-ocean ridge hydrothermal brines coupled with precipitation of solid CaCO$_3$ and SiO$_2$ phases. The more the absolute Ca^{2+} concentrations exceed these Ca^{2+} minimum estimates, the higher the likelihood that calcified cyanobacteria formed in the corresponding ocean (Fig. 3, B and C). The fossil record of calcified cyanobacteria from open-marine settings should reflect this relation (*29*) (Fig. 3D). Although the predicted and observed abundances of occurrences do not exactly coincide at the 10-Ma intervals, their rough tendencies do (Fig. 3). Above all, the predicted gaps in the Lower Permian, Lower Triassic, and Lower Jurassic apparently correspond to the Asselian, Scythian, and Toarcian, which lack marine calcified cyanobacteria, although stromatolites occur.

The most notable discrepancy exists with regard to the Cretaceous and Paleogene. Very high Ca^{2+} concentrations are suggested by the Ca^{2+} model curve of Stanley and Hardie (*2*), but fewer and fewer occurrences of calcified cyanobacteria are known from the Berriasian to Santonian (Fig. 3). However, biogenic Ca^{2+} removal is not included in the Hardie-model calculation, and the successive vanishing of calcified cyanobacteria may point to a substantial drawdown of Ca^{2+} by the calcareous nanoplankton and planktonic

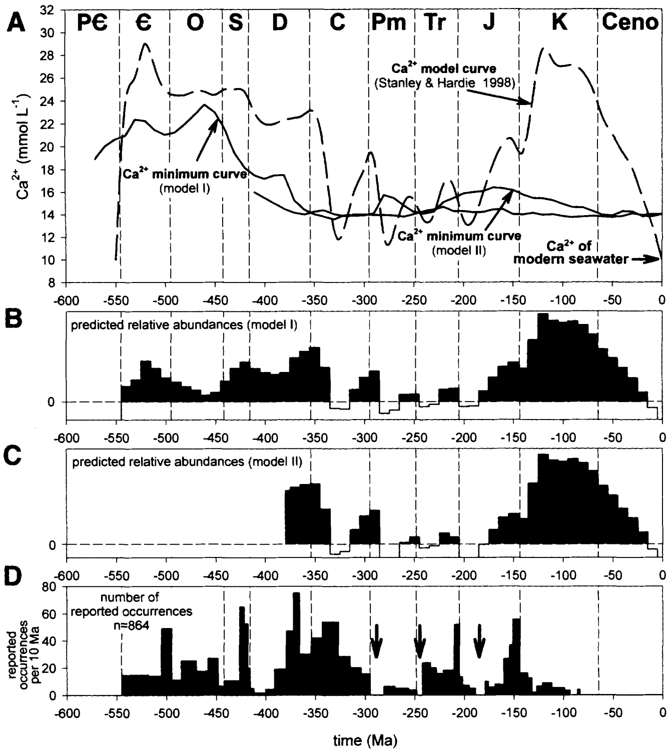

Fig. 3. (**A**) Calculated Ca^{2+} minimum curves for photosynthetically induced cyanobacterial sheath impregnation in comparison with the calculated Ca^{2+} curve of the modeling by Stanley and Hardie (*2*). Model I is based on the $p\mathrm{CO}_2$ curve of Berner (*27*), and model II on the $p\mathrm{CO}_2$ curve of Ekart *et al.* (*28*). (**B** and **C**) Predicted relative abundances of calcified marine cyanobacteria throughout the Phanerozoic based on models I and II, respectively. (**D**) Observed occurrences of calcified marine cyanobacteria on the basis of reports in 15 sedimentological-paleontological journals (*29*). The number of reported occurrences in each chronostratigraphic stage has been normalized to 10-Ma intervals. The three arrows indicate gaps in Phanerozoic occurrences.

foraminifera since the Late Jurassic (*30*). This is consistent with the volume of Upper Cretaceous–Early Paleocene chalk deposits of coccolithophorids. In the first instance, these sediments reflect high Ca^{2+} flux rates rather than high absolute Ca^{2+} concentrations.

Precambrian marine carbonate stromatolites almost completely lack calcified cyanobacteria (*8*, *9*), although cyanobacterial remains comparable to those of recent taxa were preserved upon early silification (*10*). This lack appears astonishing because most stromatolites, at least those of the Proterozoic, are considered as mineralized cyanobacteria-dominated biofilms (*9*). However, this lack can be explained by high DIC concentrations (Fig. 2). Regardless of whether high-$p\mathrm{CO}_2$ conditions ($>10^{-2}$ atm) with a slightly acidic to near-neutral ocean (*31*) or low-$p\mathrm{CO}_2$ conditions ($10^{-3.5}$ atm) with an alkaline "soda ocean" of 5 to 500 meq liter^{-1} carbonate alkalinity (*20*) are assumed, cyanobacteria could not have induced sheath calcification by photosynthetic carbon assimilation (Figs. 1 and 2). Thus, episodic Precambrian stromatolite formation should reflect exopolymer-mediated precipitation driven by physicochemical fluctuations of the whole-ocean basins. This is consistent with correlation of Proterozoic stromatolite morphotypes between different continents (*32*) and with the fractal geometry shown by some Archean stromatolites (*33*). Consequently, discoveries of 700- to 750-million-year-old calcified cyanobacteria (*34*) that unequivocally resulted from micritic sheath impregnation would set an upper limit of the $p\mathrm{CO}_2$ at 10^{-2} atm and would be consistent with a decrease in atmospheric $p\mathrm{CO}_2$ during the Late Precambrian glaciations.

Several elements of uncertainty remain. The Ca^{2+} curve of the Hardie model shifts considerably in response to changes in the mid-ocean ridge hydrothermal brine/river water ratio, although the overall shape of the curve does not change (*1*, *2*). Nevertheless, correlation with the occurrences of calcified cyanobacteria indicate that the order of magnitude of Ca^{2+} calculated by Stanley and Hardie (*2*) is, in principle, correct. Fluctuating levels of seawater $CaCO_3$ supersaturation during the Phanerozoic could be expected (*20*). However, the effect on the Ca^{2+} minimum curve is minor, because lowering of the initial SI_{Cc} of 1.0 results in higher ΔSI_{Cc} values for the settings that first show calcified cyanobacteria. Only the effect of varying temperature, Mg^{2+}, and $SO_4^{\;2-}$ concentrations (*35*) on the ΔSI_{Cc} will lead to a further modification of the Ca^{2+} minimum curve. Abundances of calcified cyanobacteria may also be influenced by the distribution of carbonate platforms or alkalinity plumes from anoxic basins (*20*). Nonetheless, the presence of calcified cyanobacteria sets a lower limit of Ca^{2+} concentration for ancient oceans, provided that hydrospheric-atmospheric $p\mathrm{CO}_2$ is known. Furthermore, the effect of carbon fixation by chemolithotrophic bacteria on carbonate precipitation should have been more significant than today during times of high seawater Ca^{2+}. This may explain the occurrence of calcareous microbial fossils such as *Renalcis* in reef cavities, and the great abundance of microbialites during large parts of the Phanerozoic. The recently discovered calcitic microbialites containing *Epiphyton*- and *Girvanella*-like structures in a hardwater lake (*36*) may therefore indeed serve as an analog for microbial reefs formed during high-Ca^{2+} times of the Paleozoic.

References and Notes

1. L. A. Hardie, *Geology* **24**, 279 (1996).
2. S. M. Stanley, L. A. Hardie, *Palaeogeogr. Palaeoclimatol. Palaeoecol.* **144**, 3 (1998).
3. P. A. Sandberg, *Nature* **305**, 19 (1983).
4. A. Pentecost, R. Riding, in *Biomineralization in Lower Plants and Animals*, B. S. C. Leadbeater, R. Riding, Eds. (Clarendon, Oxford, 1986), pp. 73–90.
5. R. Riding, *Nature* **299**, 814 (1982).
6. S. M. Awramik, *Science* **174**, 825 (1971).
7. M. R. Walter, in *Early Life on Earth*, S. Bengtson, Ed. (Columbia Univ. Press, New York, 1994), pp. 270–286.
8. R. Riding, in *Calcareous Algae and Stromatolites*, R. Riding, Ed. (Springer-Verlag, Berlin, 1991), pp. 21–51.
9. R. Riding in *Early Life on Earth*, S. Bengtson, Ed. (Columbia Univ. Press, New York, 1994), pp. 426–438.
10. A. H. Knoll, S. Golubic, in *Early Organic Evolution*, M. Schidlowski *et al.*, Eds. (Springer-Verlag, Berlin, 1992), pp. 450–462.
11. W. Stumm, J. J. Morgan, *Aquatic Chemistry* (Wiley, New York, ed. 3, 1996).
12. G. Arp, J. Hofmann, J. Reitner, *Palaios* **13**, 581 (1998).
13. G. Arp, V. Thiel, A. Reimer, W. Michaelis, J. Reitner, *Sedim. Geol.* **126**, 159 (1999).
14. G. Arp, A. Reimer, J. Reitner, *Eur. J. Phycol.* **34**, 393 (1999).
15. A. W. Decho, *Oceanogr. Mar. Biol. Annu. Rev.* **28**, 73 (1990)
16. A. Pentecost, *Geomicrobiol. J.* **4**, 285 (1985).
17. S. Mann, Ed., *Biomineralization: Chemical and Biochemical Perspectives* (VCH, Weinheim, Germany, 1989).
18. K. Simkiss, K. M. Wilbur, *Biomineralization: Cell Biology and Mineral Deposition* (Academic Press, San Diego, CA, 1989).
19. A conceptual model of EPS-mediated biofilm calcification is given in the supplementary material (*37*).
20. S. Kempe, J. Kazmierczak, *Bull. Inst. Océanogr. (Monaco) No. Spec.* **13**, 61 (1994).
21. J. B. Thompson, S. Schultze-Lam, T. J. Beveridge, D. J. Des Marais, *Limnol. Oceanogr.* **42**, 133 (1997).
22. M. U. E. Merz, *Facies* **26**, 81 (1992).
23. The photosynthesis-induced rise in supersaturation is restricted to the microenvironment within the biofilms. Further, carbon removal is actually CO_2, not $HCO_3^{\;-}$; otherwise, charge imbalance would result.
24. Photosynthesis-induced rise in supersaturation was simulated with the program PHREEQE (*37*) by substracting a given amount of 200 μmol liter^{-1} carbon from the different waters, which were all equilibrated to $SI_{Cc} = 1.0$ and $p\mathrm{CO}_2 = 10^{-3.5}$ atm. For standard seawater and freshwater, a range from high-Ca^{2+}/low-DIC to low Ca^{2+}/high-DIC waters was generated by successive addition of Ca^{2+} and DIC, respectively. Supplementary information on the model calculations and water-chemistry data of the investigated settings are provided in the supplementary material (*38*).
25. See supplementary material for DIC data and mode of cyanobacterial biofilm calcification in the different settings (*38*).
26. R. Riding, *Palaeontology* **20**, 33 (1977).
27. R. A. Berner, *Philos. Trans. R. Soc. London Ser. B* **353**, 75 (1998).
28. D. D. Ekart, T. E. Cerling, I. P. Montanez, N. J. Tabor, *Am. J. Sci.* **299**, 805 (1999).

29. The compilation is provided in the supplementary material (*38*).
30. C. D. Gebelein, in *Stromatolites*, M. R. Walter, Ed. (Elsevier, Amsterdam, 1976), pp. 499–515.
31. J. P. Grotzinger, J. F. Kasting, *J. Geol.* **101**, 235 (1993).
32. J. Bertrand-Sarfati, M. R. Walter, *Precambrian Res.* **15**, 353 (1981).
33. J. P. Grotzinger, D. H. Rothman, *Nature* **383**, 423 (1996).
34. A. H. Knoll, I. J. Fairchild, K. Swett, *Palaios* **8**, 512 (1993).
35. R. Riding, *J. Geol. Soc. London* **149**, 979 (1992).
36. B. Laval *et al.*, *Nature* **407**, 626 (2000).
37. D. L. Parkhurst, D. C. Thorstenson, L. N. Plummer, *U.S. Geol. Surv. Wat.-Res. Invest. Rep.* **80-96** (1990).
38. Supplementary data are available on *Science* Online at www.sciencemag.org/cgi/content/full/292/5522/1701/DC1.

39. We thank R. Riding and P. Westbroek for comments on an earlier draft and the Pyramid Lake Paiute Tribal Council and the Western Australian Department of Conservation and Land Management for sampling permits. Funded by the German Research Foundation and the Studienstiftung des deutschen Volkes (G.A.).

6 November 2000; accepted 10 April 2001

A Giant Sauropod Dinosaur from an Upper Cretaceous Mangrove Deposit in Egypt

Joshua B. Smith,[1]* Matthew C. Lamanna,[1] Kenneth J. Lacovara,[2]
Peter Dodson,[1,3] Jennifer R. Smith,[1] Jason C. Poole,[4]
Robert Giegengack,[1] Yousry Attia[5]

We describe a giant titanosaurid sauropod dinosaur discovered in coastal deposits in the Upper Cretaceous Bahariya Formation of Egypt, a unit that has produced three *Tyrannosaurus*-sized theropods and numerous other vertebrate taxa. *Paralititan stromeri* is the first tetrapod reported from Bahariya since 1935. Its 1.69-meter-long humerus is longer than that of any known Cretaceous sauropod. The autochthonous scavenged skeleton was preserved in mangrove deposits, raising the possibility that titanosaurids and their predators habitually entered such environments.

In the early 20th century, the Bavarian geologist Ernst Stromer described a diverse biota from the Upper Cretaceous [Cenomanian: 93.5 to 99.0 million years ago (Ma)] Bahariya Formation (*1*) of the Bahariya Oasis, Egypt (Fig. 1). The vertebrate discoveries included fish, turtles, plesiosaurs, squamates, crocodyliforms, and four dinosaurs: the theropods *Spinosaurus*, *Carcharodontosaurus*, and *Bahariasaurus*, and the sauropod *Aegyptosaurus* (*2*). Tragically, Stromer's collections were largely destroyed during an Allied bombing of Munich in 1944 (*3*). With exceptions from Morocco (*4–6*) and Algeria (*7*), evidence of Late Cretaceous African dinosaurs remains limited. An improved understanding of Late Cretaceous African terrestrial vertebrates is important for the paleoecology of this region and is needed to evaluate biogeographic hypotheses pertaining to Gondwanan fragmentation (*5*, *8–10*). Here we describe the partial skeleton of an extremely large sauropod dinosaur, the first tetrapod reported from Bahariya since 1935 (*11*). The specimen consists largely of vertebrae, pectoral girdle, and forelimb elements and is preserved in sediments indicative of intertidal deposits. A number of morphological differences distinguish the humerus of the specimen (Fig. 2A) from that of *Aegyptosaurus*, precluding referral to that genus (*12*). Because of these distinctions and its possession of several autapomorphies, we designate the new specimen as *Paralititan stromeri*, gen. et sp. nov. (*13*).

Two preserved caudal sacral centra of *Paralititan* lack pleurocoels. The centrum of the first caudal vertebra (Fig. 2B) is wider than high and procoelous, and has a convex distal articular condyle. The centrum is not biconvex, as in the titanosaurids *Alamosaurus* (*14*), *Neuquensaurus* (*14*), and *Pellegrinisaurus* (*15*). Its ventral surface has weakly developed longitudinal ridges laterally bordering a sagittal concavity. A postspinal lamina is present between spinopostzygapophyseal laminae on the distal surface of the neural spine. A second proximal caudal (Fig. 2C) is strongly procoelous and has a well-developed distal condyle.

The scapula is concave medially. A prominent dorsomedial rugosity borders the medial concavity as in the titanosaurids *Aeolosaurus*, *Lirainosaurus*, *Neuquensaurus*, and *Saltasaurus* (*14*, *16*). Distal to the glenoid, a well-developed tabular process projects from the caudoventral margin of the scapula. The development of this structure in *Paralititan* is equaled only in a scapulocoracoid referred to the brachiosaurid *Brachiosaurus altithorax* (*17*).

The humerus is strongly expanded proximally and distally. Because of the modest de-

Table 1. Phylogenetic data matrix. The macronarian *Camarasaurus* is postulated as an outgroup of titanosauriformes (*45*, *46*). Character codings are as follows: 0, hypothesized plesiomorphic states; 1 and 2, hypothesized derived states; ?, missing or uncertain data (*19*).

Taxa	Characters											
	5	10	15	20	25	30	35	40	45	50	55	
					Outgroup							
Camarasaurus	00000	00000	00000	00000	00000	00000	00000	00000	00000	00000	00000	0
					Ingroup							
Brachiosaurus brancai	11001	01000	00000	00000	00000	001?1	00000	001?0	00001	01010	01000	0
Andesaurus	??111	11000	1100?	?0?00	00??0	001??	?????	?????	?????	??111	?????	?
Epachthosaurus	??111	??010	11011	?0?01	1?011	1110?	1????	???1?	???11	111?1	?101?	0
Opisthocoelicaudia	???12	11101	?1111	1?002	01110	10111	11011	01111	11111	11101	11011	0
Alamosaurus	?????	?????	?????	??101	10011	11101	11?11	101?1	1111?	?1??1	1????	?
Malawisaurus	11?12	1???1	1100?	?0101	10011	00111	1???0	?????	?????	????1	?????	1
Paralititan	?????	?????	?????	??011	1101?	?????	??1??	?111?	???1?	?????	?????	?
Saltasaurus	??112	11111	11001	11111	11101	11101	1?111	11111	1???1	11?11	?1111	1

---

[1]Department of Earth and Environmental Science, University of Pennsylvania, 240 South 33rd Street, Philadelphia, PA 19104–6316, USA. [2]Engineering Geology, Drexel University, 3141 Chestnut Street, Philadelphia, PA 19104, USA. [3]Department of Animal Biology, School of Veterinary Medicine, University of Pennsylvania, 3800 Spruce Street, Philadelphia, PA 19104–6045, USA. [4]Academy of Natural Sciences, 1900 Ben Franklin Parkway, Philadelphia, PA 19103, USA. [5]Egyptian Geological Museum, Egyptian Geological Survey and Mining Authority, Athar El Nabi, Maadi, Cairo, Egypt.

*To whom correspondence should be addressed. E-mail: smithjb@sas.upenn.edu